ACS OMEGA

Article

http://pubs.acs.org/journal/acsodf

Ambient Pressure Hybrid Silica Monoliths with Hexamethyldisilazane: From Vitreous Hydrophilic Xerogels to Superhydrophobic Aerogels

Maria de Fátima Júlio and Laura M. Ilharco*

Centro de Química-Física Molecular and Institute of Nanoscience and Nanotechnology, Instituto Superior Técnico, Universidade de Lisboa, Avenida Rovisco Pais 1, 1049-001 Lisboa, Portugal

Supporting Information

ABSTRACT: Hybrid silica-based monoliths were synthesized at ambient pressure, using minimum amounts of the silylating agent hexamethyldisilazane (HMDZ). Depending on the synthesis approach, the materials ranged from dense and vitreous xerogels to transparent and superhydrophobic aerogels. Emphasis was given to understanding the role of the silylating agent, its content and incorporation process on the final morphology, and properties of the xerogels/aerogels. It is proven that as a coprecursor, increasing HMDZ content contributes to increase the lipophilic/hydrophilic balance, induce high surface areas, and decrease densities, but there is a maximum usable content for producing monoliths. Conversely, as a postsynthesis modifier, there is an optimum HMDZ content that maximizes hydrophobicity (water contact angle of ~144°) and induces high surface area (~700 $m^2 \cdot g^{-1}$), keeping the density low (~300 $kg \cdot m^{-3}$). It is proven that the aging period in the hydrophobizing solution is a crucial parameter. The most superhydrophobic xerogels were obtained using HMDZ as a postsynthesis modifier, achieving values of water contact angles as high as ~173°, at the cost of density increase to ~600 $kg \cdot m^{-3}$ and decrease of the surface area to ~300 $m^2 \cdot g^{-1}$. The best compromise between low density, high surface area, and superhydrophobicity is obtained using HMDZ both as a coprecursor and as a postsynthesis modifier, in a low HMDZ/tetraethoxysilane total molar ratio (<0.2), with an aging period of 16−24 h. The use of subcritical drying, along with the minimization of the expensive organic modifier quantities, allows envisaging a safe and low-cost large-scale production of a variety of materials, including superhydrophobic aerogels with potential distinctive applications.

1. INTRODUCTION

The exceptional properties of silica aerogels are responsible for the continued interest in their development, such as high specific surface area (≥1000 $m^2 \cdot g^{-1}$), very low density (3−500 $kg \cdot m^{-3}$), small pore size (1−100 nm), extremely high porosity (above 95%), very low thermal conductivity (0.01−0.02 $W \cdot m^{-1} \cdot K^{-1}$), and transparency to visible light, which allow silica aerogels to be a distinguished class of porous materials.[1,2] Both transparency and low thermal conductivity are attributed to the fine solid constituents and porous structure in the mesopore size region.[3] Given the superior assembly of properties, silica aerogels are potential candidates for a vast range of scientific and technological applications.[4−6] Despite these advantages, silica aerogels are highly susceptible to fracture or collapse of the pore structure during the drying stage and are difficult to prepare at large-scale settings because of their poor mechanical properties. Several approaches to improve the mechanical properties have been followed,[7−9] yielding silica-based products with additional capacities such as lightweight and insulating and/or shock-absorbing materials in building and transport industries, such as aeronautics and aerospace.[10−12] Controlling the hydrophobicity of silica aerogels will allow further applications in microelectronics and sensing.[13] In fact, superhydrophobic aerogels are expected to efficiently contribute to solve environmental problems, such as in oil spill cleanup operations.[14−17]

Conventionally, silica aerogels were dried above the supercritical point of the solvent, thus needing high pressures and, depending on the solvent, high temperatures.[18,19] Though once a preferred method, it is expensive, time-consuming, and often hazardous, rendering the process difficult for industrial use.[20] To commercially exploit aerogels or aerogel-like materials, cost-effective drying routes are required. By using subcritical drying, their costs are reduced and their safety is increased, partially overcoming the drawbacks.[21,22] Aerogel-like materials prepared from tetraethoxysilane (TEOS) and dried at ambient pressure, with physical properties similar to those achieved by supercritical drying, have been reported.[23]

Received: June 29, 2017
Accepted: August 14, 2017
Published: August 28, 2017

DOI: 10.1021/acsomega.7b00893
ACS Omega 2017, 2, 5060−5070

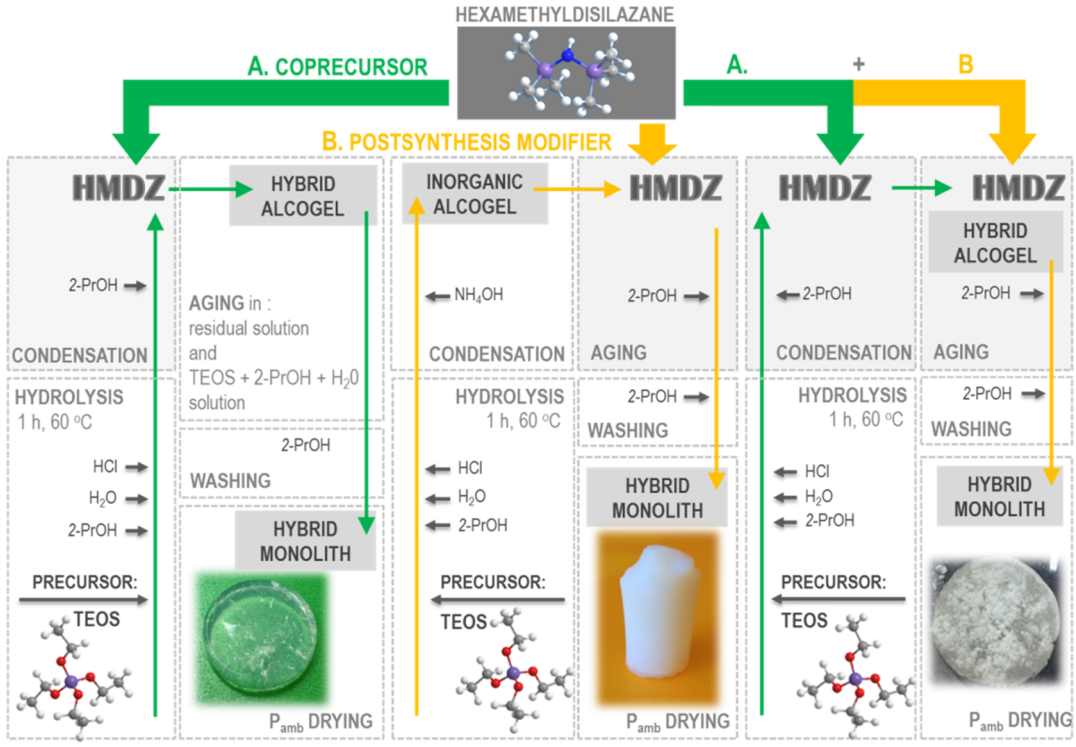

Figure 1. Scheme of the preparation of the hybrid silica aerogels.

The synthesis of hydrophobic silica aerogels has been thoroughly reviewed.[24] When drying aerogels at ambient pressure, surface modification is the key process: by introducing nonpolar groups (usually from silanes) at the surface of the pores, the capillary tensions that develop upon solvent evaporation are reduced, thus preventing pore collapse.[25]

We have recently reported the synthesis of superhydrophobic silica-based aerogels prepared from TEOS, with surface modification of the wet gel by an aging solution containing hexamethyldisilazane (HMDZ), via ambient pressure drying.[10,26]

At the same time as sylilation prevents the collapse of the silica network during drying, it hinders reactions between adjacent silica particles, thus rendering the network coarsening more difficult. Therefore, it is critical to understand the impact of the silylating agent and its incorporation process on the hybrid network.

The present work is focused on the preparation of the lightest and/or the most superhydrophobic hybrid silica aerogels at ambient pressure, by modifying the silica networks with the silylating agent HMDZ and to understand its role on the final morphology and properties of these aerogels. Hybrid monoliths are prepared by a two-step sol−gel process, with TEOS as a precursor, and different approaches are explored: using HMDZ as a coprecursor (added at the condensation step), using HMDZ as a postsynthesis modifier (in the aging solution), and using HMDZ both as a coprecursor and as a postsynthesis modifier.

When added as a coprecursor, HMDZ hydrolyzes in aqueous solution to trimethylsilanol (TMS) or to hexamethyldisiloxane (HMDS), as described by reactions 1 and 2, respectively

$$(CH_3)_3Si{-}NH{-}Si(CH_3)_3 + 2H_2O \xrightarrow{H^+} 2[(CH_3)_3Si{-}OH] + NH_3(g) \quad (1)$$

$$(CH_3)_3Si{-}NH{-}Si(CH_3)_3 + H_2O \xrightarrow{H^+} (CH_3)_3Si{-}O{-}Si(CH_3)_3 + NH_3(g) \quad (2)$$

These reactions partially neutralize the medium, thus initiating condensation and co-condensation reactions between inorganic and/or organically modified species at different stages of hydrolysis and condensation, such as

$$Si(OH)_4 + Si(OH)_4 \rightarrow (HO)_3Si{-}O{-}Si(OH)_3 + H_2O \quad (3a)$$

(slow in acidic medium,[27] it yields the first inorganic dimer that can further condense)

$$Si(OH)_4 + HO{-}Si(CH_3)_3 \rightarrow (HO)_3Si{-}O{-}Si(CH_3)_3 + H_2O \quad (3b)$$

$$(HO)_3Si{-}O{-}Si(OH)_3 + HO{-}Si(CH_3)_3 \rightarrow (HO)_3Si{-}O{-}Si[(OH)_2]{-}O{-}Si(CH_3)_3 + H_2O \quad (3c)$$

and so on, toward the organically modified silica (ORMOSIL) network.

Other condensation reactions may occur between partially hydrolyzed HMDZ, with the formation of HMDS[28]

$$(CH_3)_3Si{-}OH + HO{-}Si(CH_3)_3 \xrightarrow{H^+} (CH_3)_3Si{-}O{-}Si(CH_3)_3 + H_2O \quad (3d)$$

(slow when the concentration of the TMS species is low). If any NH_3 is still present, the reverse reactions of 1 and 2 can regenerate HMDZ.

Reactions 2 and 3d, on the other hand, consume HMDZ and TMS, respectively, which no longer contribute to the formation of the ORMOSIL network.

DOI: 10.1021/acsomega.7b00893
ACS Omega 2017, 2, 5060−5070

As a postsynthesis modifier, HMDZ reacts with the silanol groups at the surface of the pores, by the proposed overall reaction[29]

$$2\text{Si}{-}\text{OH} + (\text{CH}_3)_3\text{Si}{-}\text{NH}{-}\text{Si}(\text{CH}_3)_3 \xrightarrow{\text{H}^+} 2\text{Si}{-}\text{O}{-}\text{Si}(\text{CH}_3)_3 + \text{NH}_3 \quad (4)$$

It was proven that this is a two-step process:[30] (1) HMDZ reacts with a surface silanol to form a surface-bound trimethylsilyl and a reactive intermediate trimethylaminosilane and (2) trimethylaminosilane reacts with another surface silanol, forming a trimethylsilyl surface species and ammonia. The reaction is initially fast as nonhydrogen-bonded silanol groups, either isolated or geminal [$=\text{Si(OH)}_2$], are consumed. At longer times, it becomes slower because of hindered adsorption of HMDZ onto geminal silanols that already have one silylated hydroxyl group. Hydrogen-bonded surface vicinal silanols [$\equiv\text{Si}{-}\text{OH}\cdots\text{HO}{-}\text{Si}\equiv$] are much less available.

Once the different roles of HMDZ are understood, it is possible to envisage a synthesis procedure that maximizes superhydrophobicity or surface area or minimizes the density of the final hybrid aerogel, trying to use as minimum amounts of HMDZ as possible.

2. RESULTS AND DISCUSSION

2.1. Synthesis of Hybrid Aerogel Monoliths. The hybrid silica aerogels were synthesized as monoliths, following the procedures schematized in Figure 1.

In series A, HMDZ was used as a coprecursor. In series B, HMDZ was used only as a postsynthesis organic modifier, and in series (A + B), HMDZ was used both as a coprecursor and as a postsynthesis modifier.

The series of aerogels were synthesized by a two-step sol−gel process consisting of (1) acid-catalyzed hydrolysis of TEOS and (2) base-catalyzed polycondensation of the resulting silanol groups. In step (1), TEOS was previously diluted in 2-propanol and distilled water was added, dropwise, while stirring. The reaction mixture was acidified with 1 M HCl to initiate the hydrolysis process at pH 2.0. The acidic colloidal solution was placed in a sealed container, heated at 60 °C, with orbital stirring at 120 rpm for 60 min. In step (2), condensation was induced by adding a HMDZ solution in 2-PrOH, dropwise, with stirring at 140 rpm (series A) or by adding a NH_4OH 0.1 M aqueous solution (series B), at pH 7.0. The resulting homogeneous sols were left to gel, with no further stirring, and then allowed to age in the residual solution for 24 h.

Further aging was carried out under different conditions:

> Samples A: for a second aging period of 24 h in the residual solution, followed by washing with 2-PrOH: samples A_a, where subscript a indicates the HMDZ/TEOS molar ratio in the sample or for a second aging period of 24 h in a (TEOS + H_2O + 2-PrOH) solution, in the same proportions used in the synthesis, followed by washing with 2-PrOH: samples A'_a.
>
> Samples B: for a second aging period of variable duration in a hydrophobizing solution (HMDZ + 2-PrOH), followed by washing with 2-PrOH: samples B_b-t_x, where b refers to the HMDZ/TEOS molar ratio and x to the aging period in hours.

The properties of aerogels were optimized by using HMDZ both as a coprecursor and as a postsynthesis modifier, following the synthesis procedure of series A and the aging of series B: samples $A_a{-}B_b$-t_x, where a and b refer to the HMDZ/TEOS molar ratio added during synthesis and aging, respectively.

After aging, the pore liquid was exchanged with 2-PrOH, for washing, and the gels were dried at ambient pressure at 60 °C, in a solvent-saturated atmosphere, until their weight loss became negligible.

The photographs of some dry hybrid aerogels are shown in Figure 2.

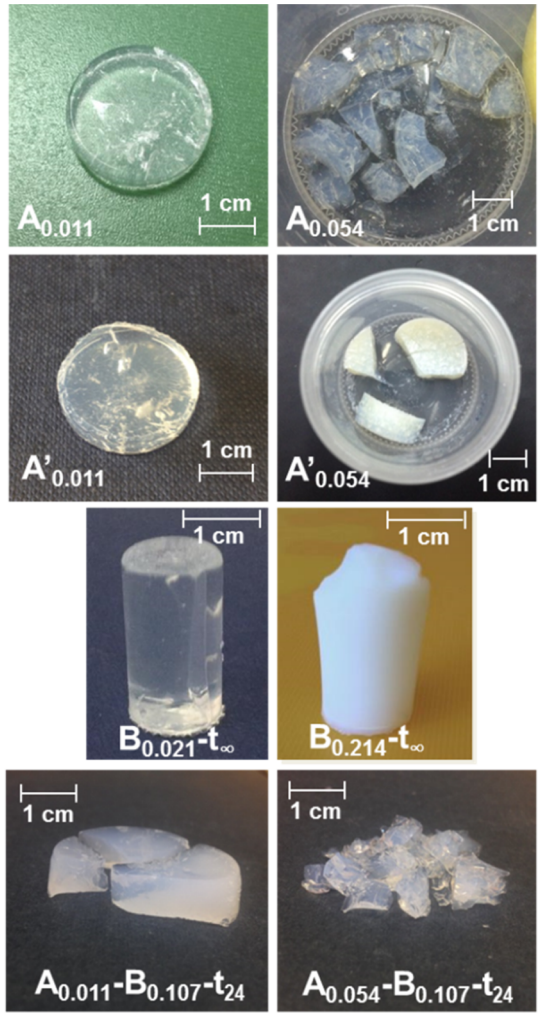

Figure 2. Photographs of ambient pressure hybrid monoliths prepared under different conditions.

The samples $A_a{-}B_b$-t_∞ and B_b-t_∞ were exceptional because hydrophobization was not stopped by washing, and the samples were left to dry in the HMDZ solution: as the solvent evaporates, the solubility product of NH_4Cl is attained, and a crystalline phase forms at the surface of the monoliths (Figure 3). It is mostly NH_4Cl, identified in the infrared spectra by the strong triply degenerate N−H deformation mode, at 1402 cm^{-1}.[31]

The samples are identified in Table 1, according to the synthesis parameters.

2.2. HMDZ as a Coprecursor. The effect of HMDZ acting as a coprecursor on the structure of the dry xerogels and aerogels was analyzed for monoliths prepared with various HMDZ/TEOS molar ratios and differing only in the aging solution (series A_a and A'_a), as described above.

DOI: 10.1021/acsomega.7b00893
ACS Omega 2017, 2, 5060−5070

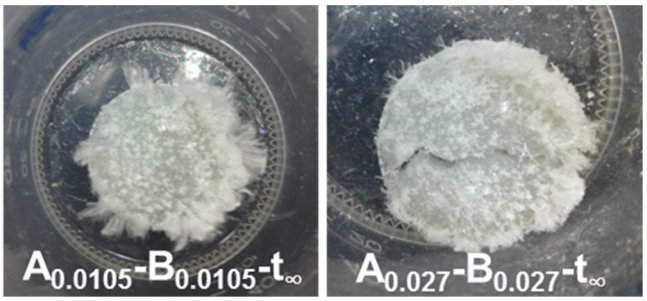

Figure 3. Photographs of ambient pressure hybrid monoliths A_a−B_b-t_∞ with a crystalline phase at the surface.

The informative region of the diffuse reflectance Fourier transform (DRIFT) spectra is compared in Figure 4.

The spectra show characteristics of hybrid silica networks, with the silica bands at ∼1078 (ν_{as}Si−O−Si), 955 (νSi−O(H)), and 802 (ν_sSi−O−Si) cm^{-1}, and the organic moiety is identified by the bands characteristic of the methyl groups of (Si)−$(CH_3)_3$ units: out-of-plane twisting modes (at 864/849 and 760 cm^{-1}). These bands are better defined, and their relative intensities increase as the HMDZ content increases. For HMDZ/TEOS = 0.054, sample $A_{0.054}$, the well-defined shoulder at 1255 cm^{-1} is assigned to the methyl symmetric deformation of trimethylsilyl groups.[32] The band related to silanol groups, νSi−O(H), clearly decreases as the content in HMDZ increases, which suggests a higher co-condensation yield (reactions 2). Above a certain HMDZ/TEOS molar ratio (0.107), the presence of the covalently bonded bulky (Si)−$(CH_3)_3$ groups starts hindering further condensation, and no monoliths are obtained.

A quantitative analysis of these spectra was carried out by deconvolution into Gaussian and Lorentzian components in the 1300−700 cm^{-1} region, using a nonlinear least squares fitting method (Figure S1 and Table S1, Supporting Information). The four Gaussian components retrieved from the bands centered at 1095−1079 cm^{-1} were assigned, taking into account the optical components of the ν_{as}Si−O−Si mode (longitudinal and transverse, respectively, LO and TO) of the most common primary siloxane units: sixfold $(SiO)_6$ and fourfold $(SiO)_4$ rings.[33] The proportion of sixfold siloxane rings was estimated from the sum of areas of the corresponding LO and TO components relative to the total area of the ν_{as}Si−O−Si band. The estimated values are summarized in Table 2 and are higher than those usually obtained for inorganic xerogels/aerogels.[34] Increasing HMDZ content results in networks richer in the less tensioned $(SiO)_6$ units, which tend to predominate as the population of the covalently bonded bulky $Si(CH_3)_3$ groups increases. This becomes clear comparing the structures obtained by energy minimization of samples $A_{0.011}$ and $A_{0.054}$ (Scheme 1), which also show that the silane groups tend to accumulate at the pores surfaces.

The lipophilic/hydrophilic balance (LHB) was estimated from the relative areas of all the CH_3-related components (Lorentzian) versus the silanol band in this region. The LHB values, summarized in Table 2, increase with the HMDZ content but are very low, indicative of hydrophilic materials. This property was confirmed by an attempt to measure the water contact angles: on samples with lower HMDZ/TEOS contents (Video S1, Supporting Information), the water droplets were instantly adsorbed, and a measure at t = 10 s was not possible.

For a certain HMDZ content, the aging solution determines the structural characteristics: for samples A'_a, the primary sixfold

Table 1. Identification of the Samples According to the Synthesis Parameters Studied

	hydrolysis (molar ratio)	condensation (molar ratio)		2nd aging stage (molar ratios)	
sample	TEOS/H_2O/2-PrOH/HCl	TEOS/HMDZ	TEOS/NH_4OH	TEOS/2-PrOH/H_2O	TEOS/HMDZ
$A_{0.011}$	1:4:8.9:0.009	1:0.011		residual solution	
$A_{0.021}$		1:0.021			
$A_{0.054}$		1:0.054			
$A'_{0.011}$		1:0.011		1:8.9:4	
$A'_{0.021}$		1:0.021			
$A'_{0.054}$		1:0.054			
$B_{0.021}$-t_∞	1:4:9:0.009		1:0.009		1:0.021
$B_{0.054}$-t_∞					1:0.054
$B_{0.107}$-t_∞					1:0.107
$B_{0.214}$-t_∞					1:0.214
$B_{0.428}$-t_∞					1:0.428
$B_{0.857}$-t_∞					1:0.857
$B_{0.214}$-t_4					1:0.214
$B_{0.214}$-t_8					
$B_{0.214}$-t_{14}					
$B_{0.214}$-t_{16}					
$B_{0.214}$-t_{24}					
$B_{0.214}$-t_{48}					
$B_{0.214}$-t_{70}					
$A_{0.0055}$−$B_{0.0055}$-t_∞	1:4:8.9:0.009	1:0.0055			1:0.0055
$A_{0.0105}$−$B_{0.0105}$-t_∞		1:0.0105			1:0.0105
$A_{0.027}$−$B_{0.027}$-t_∞		1:0.027			1:0.027
$A_{0.011}$−$B_{0.107}$-t_{24}		1:0.011			1:0.107
$A_{0.054}$−$B_{0.107}$-t_{24}		1:0.054			

DOI: 10.1021/acsomega.7b00893
ACS Omega 2017, 2, 5060−5070

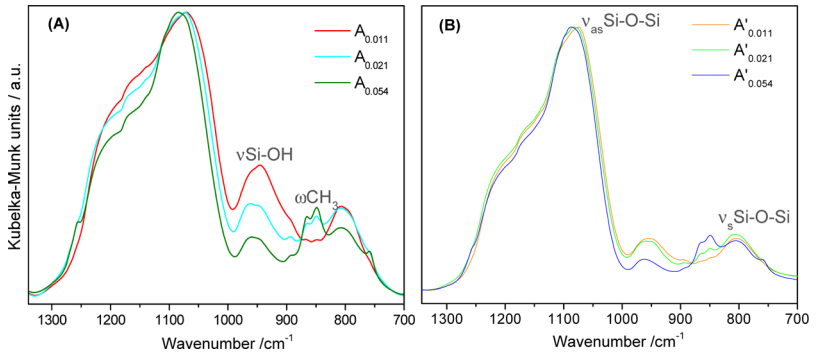

Figure 4. DRIFT spectra of hybrid monoliths using HMDZ as a coprecursor in different contents: (A) aged for 48 h in residual solution and (B) aged for 24 h in residual solution plus 24 h in (TEOS + 2-PrOH + H_2O) mixture. Spectra normalized to the ν_{as}Si−O−Si band (at ∼1078 cm^{-1}).

Table 2. Condensation pH and Gelation Times (t_g) of Aerogels Using HMDZ as a Coprecursor and Different Aging Solutions[a]

sample	condensation pH	t_g (min)	LHB[b]	% $(SiO)_6$[c]	ρ_e ($g{\cdot}cm^{-3}$)	S_{BET}[d] ($m^2{\cdot}g^{-1}$)	V_p ($cm^3{\cdot}g^{-1}$)	ϕ_{BJH}[e] (nm)
$A_{0.011}$	6	29	0.04	31.7	0.99 ± 0.02	654 ± 4	0.42	2.9
$A'_{0.011}$	6	29	0.06	29.0	0.60 ± 0.01	958 ± 2	1.17	4.8
$A_{0.021}$	7	4	0.17	44.8	0.614 ± 0.003	929 ± 5	0.99	4.1
$A'_{0.021}$	7	4	0.16	42.0	0.406 ± 0.005	902 ± 5	1.61	6.4
$A_{0.054}$	8	1.5	0.40	61.0	0.55 ± 0.01	937 ± 9	1.16	4.5
$A'_{0.054}$	8	1.5	2.61	61.0	0.376 ± 0.009	889 ± 6	1.61	6.3

[a]Structural parameters from the DRIFT spectra: LHB and fraction of six-member rings [% $(SiO)_6$]. Envelope density (ρ_e), specific surface area (S_{BET}), total pore volume (V_p) at single point p/p_0 = 0.98, and average mesopore diameter (ϕ_{BJH}) from the adsorption branch. [b]LHB = $\sum A(CH_3)/A(\nu Si{-}O(H))$, where A stands for the % area of the band. [c]% $(SiO)_6$ = 100 × $[A(LO(SiO)_6) + A(TO(SiO)_6)]/[A(LO(SiO)_6) + A(TO(SiO)_6) + A(LO(SiO)_4) + A(TO(SiO)_4)]$. [d]Determined using the Brunauer−Emmett−Teller (BET) isotherm.[36] [e]Assessed by the Barrett−Joyner−Halenda (BJH) algorithm.[37]

Scheme 1. Schematic Structure of Two Hybrid Aerogels, with the HMDZ/TEOS Molar Ratio of 0.011 (A) and 0.054 (B), Optimized by Gaussian Energy Minimization

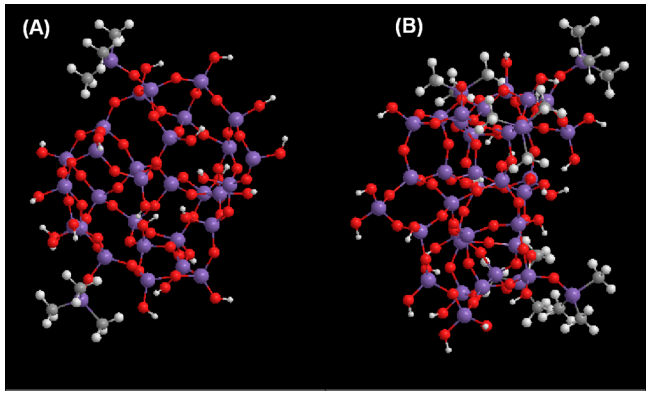

rings are less abundant, the silanol stretching components in the DRIFT spectra become relatively weaker, and the LHB becomes generally higher, consistent with less hydrophilic materials;[35] the values of the water contact angles obtained for samples $A_{0.054}$ and $A'_{0.054}$ were 21.2° and 32.5°, respectively.

Some pore morphology-related properties are also summarized in Table 2 and Figure 5 for the two series of hybrid monoliths.

The gelation times depend on the condensation pH, and thus, they vary strongly with the HMDZ/TEOS molar ratio.[27] For pH = 6 (samples $A_{0.011}$ and $A'_{0.011}$), the co-condensation reactions are slowed down and the gelation time is very long (29 min).

Aging the wet gel with the HMDZ/TEOS molar ratio of 0.011 for (24 + 24) h in the residual solution yields a dense xerogel (∼1 $g{\cdot}cm^{-3}$), with N_2 sorption isotherm characteristic of a microporous material (type I),[38] with some condensation in small mesopores (an average diameter of ∼3 nm). As the HMDZ content increases, the xerogels become lighter and mesoporous, characterized by type IV N_2 isotherms with type H2 hysteresis,[38] with decreasing density (increasing total pore volume) and increasing average mesopore dimension and surface area. The increments in all the properties attenuate as the HMDZ/TEOS molar ratio increases. Unlike most hybrid aerogels, these monoliths are transparent for the HMDZ/TEOS molar ratio below 0.054 (Figure 2) because for such low contents in the silylated groups they do not fill the pores and there is no phase separation. A similar transparency was reported by Kanamori for hybrid monoliths obtained from methyltrimethoxysilane, also dried under ambient conditions.[3,39]

The aging conditions are so important in determining the final properties of the monoliths[40] that just by changing the second 24 h aging medium to a (TEOS + 2-PrOH + water) solution, lighter (much more porous), with larger mesopores, and less hydrophilic aerogels are obtained (series A'_a). In this case, all samples exhibit type IV N_2 isotherms with H2 hysteresis loops (Figure 5A), characteristic of mesoporous materials. The condensation reactions that occur during the second aging period strengthen the silica network, reducing shrinkage upon drying.[41] By comparing the properties of samples $A'_{0.021}$ and $A'_{0.054}$, it is obvious that the differences fade out as the HMDZ content increases, suggesting that it is not necessary to use a high content of HMDZ as a coprecursor to obtain hybrid aerogel-like monoliths, once appropriate aging conditions are chosen. Conversely, even these low HMDZ contents reflect in a significant way on the structure of the hybrid monoliths.

DOI: 10.1021/acsomega.7b00893
ACS Omega 2017, 2, 5060−5070

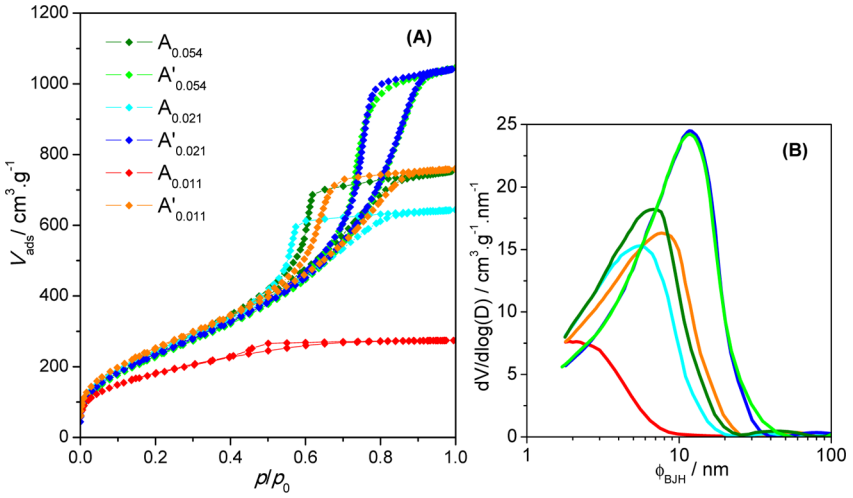

Figure 5. (A) N_2 adsorption−desorption isotherms of aerogels using HMDZ as a coprecursor and different aging solutions and (B) mesopore size distribution from the BJH analysis of the adsorption branch for samples A_a and A'_a.

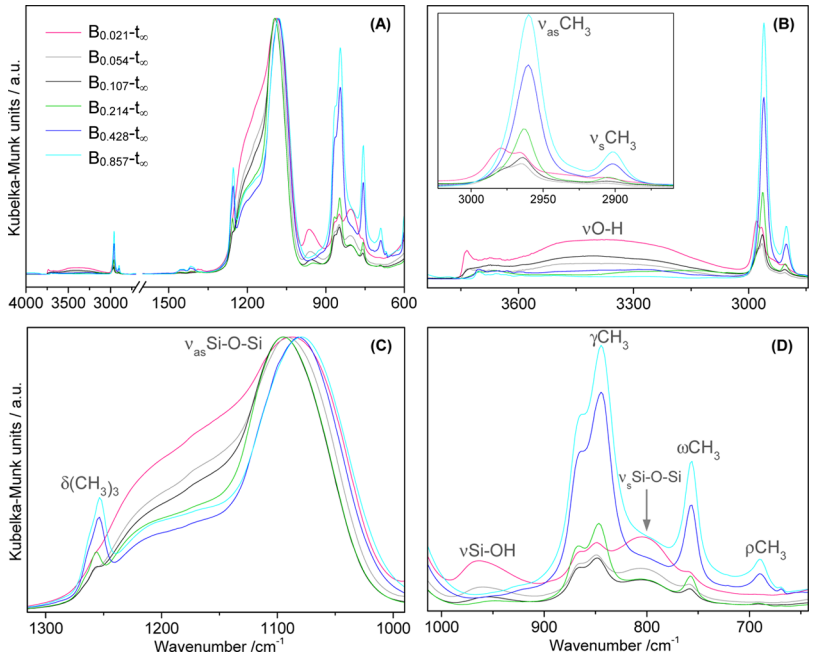

Figure 6. (A) DRIFT spectra of modified aerogels (samples B_b-t_∞), normalized to the ν_{as}Si−O−Si band (at ∼1090 cm^{-1}) and (B−D) enhanced spectral regions.

2.3. HMDZ as a Postsynthesis Modifier. When HMDZ acts as only a postsynthesis modifier (samples B_b-t_x), the structure of the final aerogel depends on the HMDZ content in the aging solution and on the aging period.

The first effect of the increasing HMDZ content is the transition from transparent to translucent and then to opaque monoliths (Figure 2). The DRIFT spectra of monoliths left to dry without washing (Figure 6) allow to understand the drastic effects of the HMDZ concentration on the structure of the dry aerogels: the bands assigned to the vibrational modes of the nonequivalent methyl groups of trimethylsilyl units, such as antisymmetric and symmetric stretching (at 2964 and 2900 cm^{-1}), antisymmetric and symmetric deformation (at 1440/1417 and 1253 cm^{-1}), out-of-plane twisting (at 863/844 and 756 cm^{-1}), and rocking (at 690 cm^{-1}), increase with the HMDZ content, in a clear sign of a more efficient hydrophobization of the network. The slight shifts in comparison to the spectra of series A_a are due to the trimethylsilyl groups remaining exclusively at the surface of the pores in a more nonpolar environment. For the lowest HMDZ content (sample $B_{0.021}$-t_∞), some of these bands appear to be stronger, but this is due to the overlapping with silica bands, namely, ν_sSi−O−Si (at 800 cm^{-1}). Simultaneously, some effects are induced on the inorganic network by hydrophobization: the ν_{as}Si−O−Si band shifts to lower wavenumbers (from 1095 to 1079 cm^{-1}) and becomes narrower. With increasing content in HMDZ in the aging solution, the network loses silanol groups (more complete condensation): the relative intensities of the broad bands at ∼3300 cm^{-1} (νO−H, hydrogen bonded), 3600 cm^{-1} (νO−H of free groups), and 950 cm^{-1} (νSi−O(H)/νSiO$^-$) decrease.

The proportion of sixfold siloxane rings and the LHB were estimated from the quantitative analysis of the spectra in the

DOI: 10.1021/acsomega.7b00893
ACS Omega 2017, 2, 5060−5070

Table 3. Summary of the Structural Properties Assessed by Deconvolution of the DRIFT Spectra in the Spectral Region between 1300 and 700 cm^{-1} for Monoliths Prepared with HMDZ as a Postsynthesis Modifier[a]

	sample					
	$B_{0.021}$-t_∞	$B_{0.054}$-t_∞	$B_{0.107}$-t_∞	$B_{0.214}$-t_∞	$B_{0.428}$-t_∞	$B_{0.857}$-t_∞
$\sum A(CH_3)$	6.5	6.7	7.0	11.1	22.8	27.9
$\sum A(Si{-}OH/Si{-}O^-)$	3.9	2.3	1.0			
LHB[b]	1.6	2.7	6.2			
% $(SiO)_6$[c]	28.6	47.2	55.2	59.9	64.1	66.4
θ (deg)	28.1	47.5	143.8	154.0	165.5	172.8

[a]Corresponding water contact angles (θ). [b]LHB = $\sum A(CH_3)/\sum A(\nu Si{-}O(H))$, where A stands for the % area of the band. [c]% $(SiO)_6$ = 100 × $[A(LO(SiO)_6) + A(TO(SiO)_6)]/[A(LO(SiO)_6) + A(TO(SiO)_6) + A(LO(SiO)_4) + A(TO(SiO)_4)]$.

1300−700 cm^{-1} region (Figure S2 and Table S2, Supporting Information). The results are summarized in Table 3.

The hydrophobization success is proved by the increase in the relative areas of the CH_3-related modes with the HMDZ content, associated with the decrease in the silanol-related components (decrease in hydrophilicity), which become negligible for the HMDZ/TEOS ratio ≥0.214. These evolutions bring about a drastic increase in LHB. The water contact angles support that these hybrid monoliths range from hydrophilic to superhydrophobic as the HMDZ content increases (Table 3 and Video S2, Supporting Information). This property assures a high stability of these aerogels at atmospheric moisture and broadens the scope of applications. The percentage in six-member siloxane rings increases with hydrophobization, probably because of breaking of some siloxane bridges in the more tensioned four-member rings as the silylation reactions occur, with conversion to the sixfold units.

The HMDZ concentration also influences the envelope density and the pore structure of the hybrid aerogels, as evidenced in Table 4 and Figure 7.

Table 4. Envelope Density (ρ_e), Specific Surface Area (S_{BET}), Parameter C (from the BET Equation), Total Pore Volume (V_p) at Single Point p/p_0 = 0.98, and Average Mesopore Diameter (ϕ_{BJH}) from the Adsorption Branch for Monoliths Prepared with Different HMDZ Contents as a Postsynthesis Modifier

sample	ρ_e ($g{\cdot}cm^{-3}$)	S_{BET} ($m^2{\cdot}g^{-1}$)	C_{BET}[a]	V_p ($cm^3{\cdot}g^{-1}$)	ϕ_{BJH} (nm)
$B_{0.021}$-t_∞	0.418 ± 0.006	671 ± 3	34	1.59	8.0
$B_{0.054}$-t_∞	0.349 ± 0.004	783 ± 6	29	1.76	7.5
$B_{0.107}$-t_∞	0.308 ± 0.003	715 ± 8	16	1.93	8.6
$B_{0.214}$-t_∞	0.370 ± 0.004	771 ± 8	21	1.63	6.9
$B_{0.428}$-t_∞	0.403 ± 0.006	593 ± 7	14	1.50	7.7
$B_{0.857}$-t_∞	0.603 ± 0.007	379 ± 3	18	0.79	6.4

[a]p/p_0 range for applicability of the BET equation: 0.06−0.27.

Two opposite effects are induced by HMDZ: the springback that occurs upon drying because of the presence of the methyl groups at the surface of the pores is responsible for a decrease in density; on the other hand, as the HMDZ content increases, more numerous bulky groups ($-Si-(CH_3)_3$) fill the pores. Thus, the density presents a minimum at a certain value of the HMDZ concentration (sample $B_{0.107}$-t_∞).

These results are confirmed by the nitrogen adsorption−desorption results (Figure 7): the isotherms are all type IV with H2 hysteresis typical of mesoporous materials, but the total pore volume increases with the HMDZ content up to a maximum for sample $B_{0.107}$-t_∞. This particular isotherm is slightly different, as the plateau for high pressures is not well-defined, suggesting a population of larger mesopores, confirmed by the mesopore size distribution (Figure 7B), or even of macropores.[38] In this sample, all the data point to a more open structure because of the repulsive effect between organic groups prevailing over the filling of the pores. The infrared spectra in the $\nu_{as}CH_3$ region corroborate this effect: the degenerate $\nu_{as}CH_3$ band has two components for very low HMDZ content, at 2980 and 2964 cm^{-1} (observed for samples $B_{0.021}$-t_∞ and $B_{0.054}$-t_∞ in Figure 5B), the first one initially stronger, inverting for sample $B_{0.054}$-t_∞. Above this content only the lower wavenumber component appears, corresponding to the methyl groups that fill the pores. The unrelated oscillations of the average mesopore size in the range of 6.4−8.6 nm (estimated from the adsorption branch, using the BJH algorithm) and of the specific surface area in the range of ∼380 to ∼780 $m^2{\cdot}g^{-1}$ (from the BET equation) are indicative of a change in the pore shape as the pores become more filled with organic groups.

The optimum HMDZ content in the aging solution will depend on whether the aim is to obtain the lightest or the most superhydrophobic hybrid aerogel.

It is expectable that for a given HMDZ content, the aging period also influences the possibility of obtaining lighter hybrid aerogels. This time effect was studied for samples with a HMDZ content that assures a very high hydrophobicity ($B_{0.214}$-t_x), by varying the aging period between 4 h and t_∞ (Figure 8).

The minimum envelope density (ρ_e = 0.305 $g{\cdot}cm^{-3}$) was obtained by aging the monolith for a period of 16 h in a HMDZ solution corresponding to the HMDZ/TEOS molar ratio of 0.214, but the sample is barely hydrophobic. As the aging period is prolonged, a gain in hydrophobicity is accompanied by an increase in density. At ∼60 h, superhydrophobicity is attained and aerogel-like monoliths are obtained, with an envelope density of ∼0.365 $g{\cdot}cm^{-3}$. There is no need for longer aging periods because stabilization is reached.

The above results prove that for optimizing the low-density/superhydrophobicity binomial there is no need to use a high HMDZ content or a long aging period. This is consistent with the proposed mechanism for silylation, according to which the reaction is expected to slow down with time as HMDZ diffuses to geminal silanol groups already partially silylated.[30] It is also convenient from the industrial viewpoint that tends to favor short aging periods.[40]

2.4. HMDZ Both as a Coprecursor and as a Postsynthesis Modifier. The total HMDZ/TEOS molar ratios employed were comparable to those used separately as coprecursor and as modifier (0.011, 0.021, and 0.054) but half added at the condensation stage and half in the aging solution. The total molar ratio of 0.054 was not exceeded,

DOI: 10.1021/acsomega.7b00893
ACS Omega 2017, 2, 5060−5070

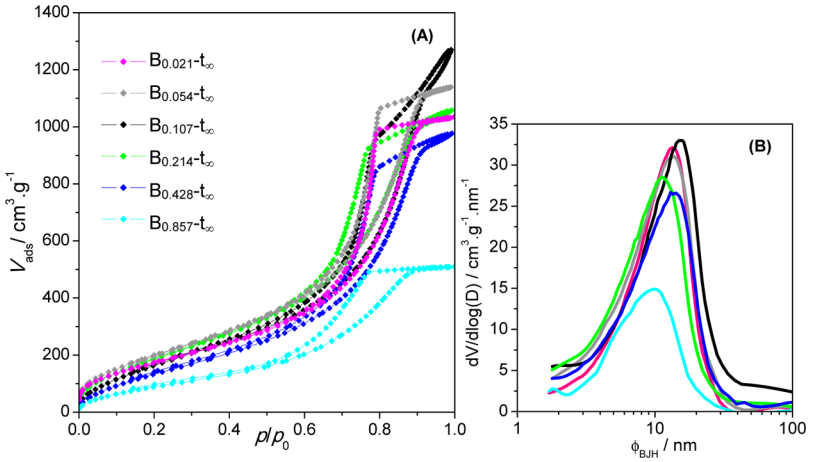

Figure 7. (A) N_2 adsorption−desorption isotherms of modified inorganic aerogels and (B) corresponding mesopore size distribution from the BJH analysis of the adsorption branch for samples B_b-t_∞.

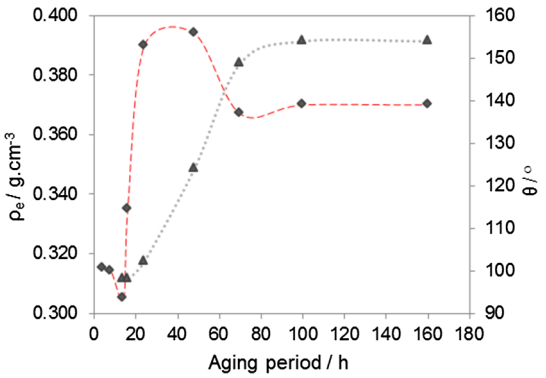

Figure 8. Envelope densities (♦) and water contact angles (▲) of sample $B_{0.214}$-t_x as a function of the aging period.

because it assures the formation of monoliths when HMDZ acts only as coprecursor: samples $A_{0.0055}$−$B_{0.0055}$-t_∞, $A_{0.0105}$−$B_{0.0105}$-t_∞, and $A_{0.027}$−$B_{0.027}$-t_∞. The samples were left to dry without washing (second aging period of t_∞) to assure that the total HMDZ remained in the gel.

Figure 9 and Table 5 condense the structural information of these samples and compare them with those obtained for the same HMDZ content as a coprecursor and as a modifier.

As expected, the evolution of the relative intensities of the methyl related bands follows the HMDZ total content, namely, in the bands at 863/844 and 756 cm^{-1} (Figure 9A inset). The quantitative analysis of these spectra in the 1300−700 cm^{-1} region (Figure S3 and Table S3, Supporting Information) confirmed this conclusion because the estimated LHB increases from 1.2 to 4.7 as the total HMDZ/TEOS molar ratio varies from 0.011 to 0.054 (Table 5). The water contact angles correlate well (27.5°−141.0°), showing that these hybrid monoliths range from hydrophilic to very hydrophobic, accompanied by a decrease in the envelope density. Comparison with the properties of monoliths prepared using the same total amount of HMDZ but only as a coprecursor (samples A_a) or only as a postsynthesis modifier (samples B_b) is also relevant: in terms of hydrophobicity (LHB and water contact angle), HMDZ in the double role (series A_a−B_b) is advantageous, as the organic groups already bonded to the network facilitate diffusion of the hydrophobizing bath, and so, the same total amount of HMDZ has a higher silylation yield. The same is not true in terms of density because the monoliths of series A_a−B_b are lighter than those of series A_a but denser than the corresponding ones of series B_b. Thus, the amount used as a coprecursor contributes to denser xerogels, only partially compensated by the aging in HMDZ solution.

The N_2 isotherms (Figure 9B) and the morphological values obtained from them (Table 5) highlight that for a similar aging

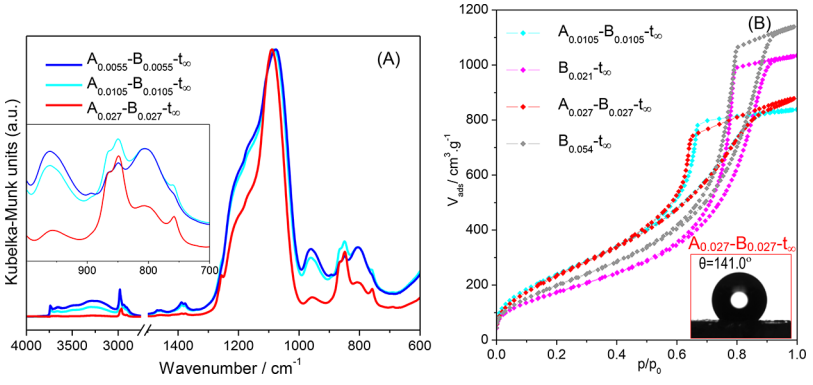

Figure 9. (A) DRIFT spectra of hybrid monoliths normalized to the ν_{as}Si−O−Si band (at ∼1090 cm^{-1}); inset—enhanced low wavenumber spectral region; (B) N_2 isotherms of samples A_a−B_b and A_0−B_b with the same total amount of HMDZ; inset—water contact angle for the most hydrophobic sample in this series: $A_{0.027}$−$B_{0.027}$-t_∞.

DOI: 10.1021/acsomega.7b00893
ACS Omega 2017, 2, 5060−5070

Table 5. Envelope Density (ρ_e), Specific Surface Area (S_{BET}), Total Pore Volume (V_p) at Single Point p/p_0 = 0.98, Average Mesopore Diameter (ϕ_{BJH}), Water Contact Angle (θ), and LHB of Sample A_a−B_b-t_∞[a]

sample	ρ_e (g·cm^{-3})	S_{BET} (m^2·g^{-1})	V_p (cm^3·g^{-1})	ϕ_{BJH} (nm)	θ (deg)	LHB
$A_{0.0055}$−$B_{0.0055}$-t_∞	0.512 ± 0.006	1071 ± 4	1.28	4.6	27.5	1.2
$A_{0.0105}$−$B_{0.0105}$-t_∞	0.472 ± 0.006	934 ± 7	1.29	5.0		1.6
$A_{0.027}$−$B_{0.027}$-t_∞	0.451 ± 0.006	923 ± 6	1.30	5.0	141.0	4.7
$A_{0.011}$	0.997 ± 0.018	654 ± 4	0.42	2.9		0.04
$A_{0.021}$	0.614 ± 0.003	929 ± 5	0.99	4.1		0.17
$A_{0.054}$	0.551 ± 0.010	937 ± 9	1.16	4.5	21.2	0.40
$B_{0.021}$-t_∞	0.418 ± 0.006	671 ± 3	1.59	8.0	28.1	1.6
$B_{0.054}$-t_∞	0.349 ± 0.004	783 ± 6	1.76	7.5	47.5	2.7

[a]For comparison, samples A_a and B_b-t_∞ are also included.

Table 6. Envelope Density (ρ_e), Specific Surface Area (S_{BET}), Total Pore Volume (V_p) at Single Point p/p_0 = 0.98, Average Mesopore Diameter (ϕ_{BJH}), Water Contact Angle (θ), and LHB of Samples A_a−$B_{0.107}$-t_{24}[a]

sample	ρ_e (g·cm^{-3})	S_{BET} (m^2·g^{-1})	V_p (cm^3·g^{-1})	ϕ_{BJH} (nm)	θ (deg)	LHB
$A_{0.011}$−$B_{0.107}$-t_{24}	0.410 ± 0.009	1013 ± 7	1.36	4.9	143.9	5.1
$A_{0.054}$−$B_{0.107}$-t_{24}	0.409 ± 0.006	968 ± 6	1.56	5.7	151.1	7.3
$B_{0.214}$-t_{24}	0.397 ± 0.003	777 ± 8	2.2	9.1	102.2	3.8

[a]For comparison, sample $B_{0.214}$-t_{24} is also included.

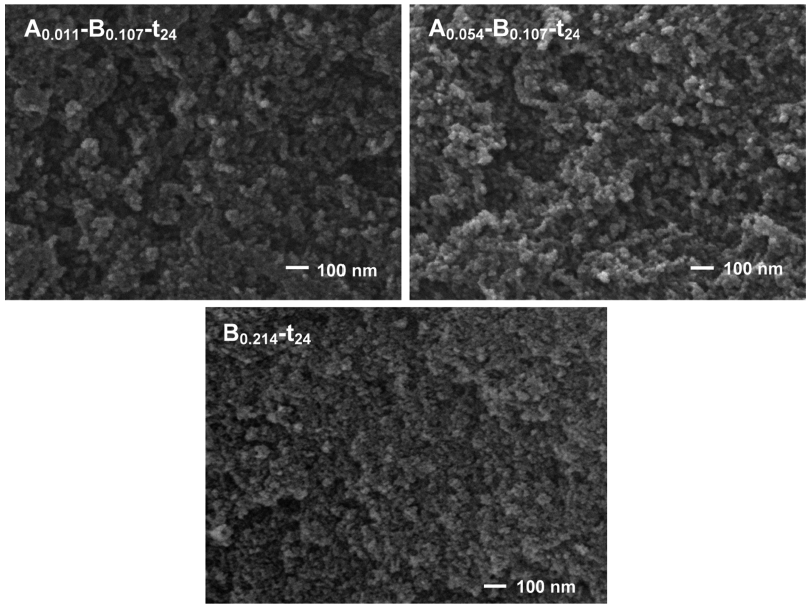

Figure 10. SEM images for samples A_a−$B_{0.107}$-t_{24}, as indicated, and sample $B_{0.214}$-t_{24}.

solution, the pore structure of the resulting aerogel is determined by its wet network whether it is hybrid or inorganic, as shown by comparison of samples $A_{0.027}$−$B_{0.027}$ and $B_{0.021}$: the total pore volume and average pore dimension are higher and the surface area is lower when the wet gel is inorganic.

Comparison of samples with the same total HMDZ content ($A_{0.0105}$−$B_{0.0105}$ and $B_{0.021}$ or $A_{0.027}$−$B_{0.027}$ and $B_{0.054}$) shows that using all the HMDZ as a postsynthesis modifier results in a lighter hybrid network with a higher total pore volume, larger pores, and thus lower surface areas. This is due to a stronger silylation effect of a more concentrated solution.

On the basis of the above observations, an approach for preparing A_a−B_b monoliths was followed, which maximizes hydrophobicity and specific surface area without a significant increase in density: the aging solution that yields minimum density in series B_b was used to silylate hybrid networks with various HMDZ contents and for a period of ∼24 h (samples $A_{0.011}$−$B_{0.107}$-t_{24} and $A_{0.054}$−$B_{0.107}$-t_{24}).

The structural and physical properties derived from the infrared spectra and nitrogen isotherms (Figures S4 and S5, Supporting Information) are compared in Table 6.

The envelope densities are similar to those of samples obtained using a higher HMDZ content as a postsynthesis modifier for 24 h and are almost insensitive to the HMDZ content as a coprecursor. The prevailing effect of HMDZ on the envelope density is thus as surface modifier. Nevertheless, a striking improvement is achieved in terms of superhydrophobicity and specific surface area of the monoliths using HMDZ in the double role.

The pore structure is also influenced by the role and content of HMDZ: the N_2 isotherm of sample $A_{0.054}$−$B_{0.107}$-t_{24} (Figure S4B, Supporting Information) rises rapidly near p/p_0 = 1, indicating the presence of macropores that contribute to a

DOI: 10.1021/acsomega.7b00893
ACS Omega 2017, 2, 5060−5070

higher total pore volume, with a decrease in specific surface area.[38] The scanning electron microscopy (SEM) images (Figure 10) confirm a more open and three-dimensional structure of this sample on the macropore scale.

On the other hand, sample $B_{0.214}$-t_{24} owes the higher total pore volume and lower surface area to a larger average dimension of the mesopores. Apparently, when HMDZ acts as a postsynthesis modifier on a wet structure that has already a large content in silyl groups, macropores tend to form and remain upon subcritical drying.

3. CONCLUSIONS

Transparent hybrid silica-based monoliths dried at ambient pressure were synthesized using minimum amounts of an organic modifier (HMDZ), ranging from vitreous and dense xerogels to superhydrophobic aerogels. HMDZ may act as a coprecursor, as a postsynthesis modifier, or as both.

When HMDZ acts only as a coprecursor, high-density hydrophilic xerogels with high specific surface areas are obtained. Low contents must be used because for HMDZ/TEOS molar ratios ≥0.107 the gels flocculate, resulting in powders instead of monoliths. When HMDZ acts as a postsynthesis modifier, superhydrophobic aerogels are obtained. For each HMDZ/TEOS molar ratio, correlations between the aging period in the silylating solution and density or hydrophobicity were established. The effect of aging in a hydrophobizing solution until complete drying is twofold: the trimethylsilyl groups that remain attached to the surface of the pores contribute not only to increase hydrophobicity but also to increase the density of the gel. However, if the pore liquid is replaced by solvent after 24 h, hydrophobization is efficient, but the entrapped organic molecules are removed and much lighter gels are resulted. Advantage may be taken from the best of each role using HMDZ both as a coprecursor and as a postsynthesis modifier, to obtain superhydrophobic aerogels with high specific surface areas.

The synthesis procedure may be adjusted, depending on whether the emphasis is on lowering the density, increasing the surface area, or maximizing superhydrophobicity. The intended applications will thus dictate the procedure to follow.

4. MATERIALS AND METHODS OF CHARACTERIZATION

TEOS (98%) from Aldrich was used as a silica precursor, 2-propanol p.a. from Sigma-Aldrich as a solvent, HCl (1 M) p.a. from CARLO ERBA and NH_4OH (0.1 M) p.a. from Merck as catalysts, and HMDZ (99.9%) from Aldrich as a coprecursor and/or an organic modifier.

The molecular structure of the hybrid aerogels was studied by Fourier transform infrared (FTIR) spectroscopy in a diffuse reflectance mode (DRIFT), using a Mattson FTIR spectrometer with a Specac Selector, in the range of 4000−400 cm^{-1} (wide-band mercury cadmium telluride detector), at 4 cm^{-1} resolution. The spectra were the result of rationing 500 added scans for each sample against the same number of scans for the background (grinded KBr).

The pore structure was analyzed by N_2 adsorption−desorption isotherms at 77 K of the degassed samples, using a Micromeritics ASAP 2020 instrument. The degassing programs consisted of evacuation (10 mbar) for 60 min at 30 °C and heating for 1200 min at 40 °C. The volume of nitrogen adsorbed between two consecutive points was 15 $cm^3 \cdot g^{-1}$.[42] The total time per run varied between 24 and 130 h.

The morphology of the hybrid aerogel monoliths was observed by a Scanning Electron Microscopy (SEM). The SEM images were recorded on a FEG-SEM JEOL JSM-7001F instrument operated at an accelerating voltage of 10 keV. The surfaces of the samples were sputter-coated with gold prior to analysis.

The envelope densities of the monolithic aerogels were measured with a GeoPyc 1360 instrument by Micromeritics, using a consolidation force of 15 N for 15 measurement cycles. The samples were previously degassed.

The water contact angle measurements were performed at room temperature (22 °C) by placing water droplets (5 μL) on the aerogel surface and taking several close-up photographs with a Casio EX-F1 EXILIM Pro camera. The contact angle measurements were obtained from the snapshots using ImageJ 1.45 software.

■ ASSOCIATED CONTENT

Supporting Information

The Supporting Information is available free of charge on the ACS Publications website at DOI: 10.1021/acsomega.7b00893.

Deconvolution of the infrared spectra in the 1300−700 cm^{-1} region for all the samples; components obtained by deconvolution of the spectral region between 1300 and 700 cm^{-1} for all the samples; and DRIFT spectra and N_2 sorption isotherms of samples A_a−$B_{0.107}$-t_{24} (PDF)

Water contact angle on a hydrophilic xerogel surface (AVI)

Water contact angle on a hydrophobic aerogel surface (the water droplet tends to slide) (AVI)

■ AUTHOR INFORMATION

Corresponding Author

*E-mail: lilharco@tecnico.ulisboa.pt (L.M.I.).

ORCID

Laura M. Ilharco: 0000-0001-6994-1464

Notes

The authors declare no competing financial interest.

■ ACKNOWLEDGMENTS

This work was supported by Fundação para a Ciência e a Tecnologia (FCT), project UID/NAN/50024/2013. M.d.F.J.'s PhD grant (SFRH/BDE/112796/2015) from FCT and Saint-Gobain-Weber Portugal is gratefully acknowledged.

■ REFERENCES

(1) Pierre, A. C.; Rigacci, A. SiO_2 aerogels. In *Aerogels Handbook*; Aegerter, M. A., et al., Eds.; Springer Science+Business Media: New York, 2011; pp 21−45.

(2) Zhao, S. Aerogels. In *The Sol-Gel Handbook: Synthesis, Characterization and Applications*; Levy, D., Zayat, M., Eds.; Wiley VCH: Weinheim, 2015; pp 519−574.

(3) Kanamori, K. Hybrid Aerogels. In *Handbook of Sol-Gel Science and Technology*; Klein, L., et al., Eds.; Springer International Publishing: Switzerland, 2016; pp 1−22.

(4) Pierre, C. A.; Pajonk, M. G. Chemistry of aerogels and their applications. *Chem. Rev.* **2002**, *102*, 4243−4265.

(5) Maleki, H.; Durães, L.; García-González, C. A.; del Gaudio, P.; Portugal, A.; Mahmoudi, M. Synthesis and biomedical applications of aerogels: Possibilities and challenges. *Adv. Colloid Interface Sci.* **2016**, *236*, 1−27.

DOI: 10.1021/acsomega.7b00893
ACS Omega 2017, 2, 5060−5070

(6) Martinez, R. G.; Goiti, E.; Reichenauer, G.; Zhao, S.; Koebel, M.; Barrio, A. Thermal assessment of ambient pressure dried silica aerogel composite boards at laboratory and field scale. *Energy Build.* **2016**, *128*, 111−118.
(7) Maleki, H.; Durães, L.; Portugal, A. An overview on silica aerogels synthesis and different mechanical reinforcing strategies. *J. Non-Cryst. Solids* **2014**, *385*, 55−74.
(8) Fidalgo, A.; Farinha, J. P. S.; Martinho, J. M. G.; Ilharco, L. M. Flexible hybrid aerogels prepared under subcritical conditions. *J. Mater. Chem. A* **2013**, *1*, 12044−12052.
(9) Ciriminna, R.; Fidalgo, A.; Pandarus, V.; Béland, F.; Ilharco, L. M.; Pagliaro, M. The sol−gel route to advanced silica-based materials and recent applications. *Chem. Rev.* **2013**, *113*, 6592−6620.
(10) de Fátima Júlio, M.; Soares, A.; Ilharco, L. M.; Flores-Colen, I.; de Brito, J. Silica-based aerogels as aggregates for cement-based thermal renders. *Cem. Concr. Compos.* **2016**, *72*, 309−318.
(11) Randall, J. P.; Meador, M. A. B.; Jana, S. C. Tailoring mechanical properties of aerogels for aerospace applications. *ACS Appl. Mater. Interfaces* **2011**, *3*, 613−626.
(12) Strobach, E.; Bhatia, B.; Yang, S.; Zhao, L.; Wang, E. N. High temperature annealing for structural optimization of silica aerogels in solar thermal applications. *J. Non-Cryst. Solids* **2017**, *462*, 72−77.
(13) Wang, C.-T.; Wu, C.-L.; Chen, I.-C.; Huang, Y.-H. Humidity sensors based on silica nanoparticle aerogel thin films. *Sens. Actuators, B* **2005**, *107*, 402−410.
(14) de Fátima Júlio, M.; Ilharco, L. M. Superhydrophobic hybrid aerogel powders from waterglass with distinctive applications. *Microporous Mesoporous Mater.* **2014**, *199*, 29−39.
(15) Rao, A. V.; Pajonk, G. M.; Nadargi, D. Y.; Koebel, M. M. Superhydrophobic and flexible Aerogels. In *Aerogels Handbook*; Aegerter, M. A., et al., Eds.; Springer Science+Business Media: New York, 2011; pp 79−101.
(16) Perdigoto, M. L. N.; Martins, R. C.; Rocha, N.; Quina, M. J.; Gando-Ferreira, L.; Patrício, R.; Durães, L. Application of hydrophobic silica based aerogels and xerogels for removal of toxic organic compounds from aqueous solutions. *J. Colloid Interface Sci.* **2012**, *380*, 134−140.
(17) Qin, G.; Yao, Y.; Wei, W.; Zhang, T. Preparation of hydrophobic granular silica aerogels and adsorption of phenol from water. *Appl. Surf. Sci.* **2013**, *208*, 806−811.
(18) Błaszczyński, T.; Ślosarczyk, A.; Morawski, M. Synthesis of silica aerogel by supercritical drying method. *Procedia Eng.* **2013**, *57*, 200−206.
(19) García-González, C. A.; Camino-Rey, M. C.; Alnaief, M.; Zetzl, C.; Smirnova, I. Supercritical drying of aerogels using CO_2: Effect of extraction time on the end material textural properties. *J. Supercrit. Fluids* **2012**, *66*, 297−306.
(20) Dowson, M.; Grogan, M.; Birks, T.; Harrison, D.; Craig, S. Streamlined life cycle assessment of transparent silica aerogel made by supercritical drying. *Appl. Energy* **2012**, *97*, 396−404.
(21) Aravind, P. R.; Shajesh, P.; Soraru, G. D.; Warrier, K. G. K. Ambient pressure drying: a successful approach for the preparation of silica and silica based mixed oxide aerogels. *J. Sol-Gel Sci. Technol.* **2010**, *54*, 105−117.
(22) Wang, J.; Wei, Y.; He, W.; Zhang, X. A versatile ambient pressure drying approach to synthesize silica-based composite aerogels. *RSC Adv.* **2014**, *4*, 51146−51155.
(23) Sarawade, P. B.; Kim, J.-K.; Kim, H.-K.; Kim, H.-T. High specific surface area TEOS-based aerogels with large pore volume prepared at an ambient pressure. *Appl. Surf. Sci.* **2007**, *254*, 574−579.
(24) Anderson, A. M.; Carroll, M. K. Hydrophobic silica aerogels: review of synthesis, properties and applications. In *Aerogels Handbook*; Aegerter, M. A., et al., Eds.; Springer Science+Business Media: New York, 2011; pp 47−77.
(25) Li, M.; Jiang, H.; Xu, D.; Hai, O.; Zheng, W. Low density and hydrophobic silica aerogels dried under ambient pressure using a new co-precursor method. *J. Non-Cryst. Solids* **2016**, *452*, 187−193.
(26) de Fátima Júlio, M.; Soares, A.; Ilharco, L. M.; Flores-Colen, I.; de Brito, J. Aerogel-based renders with lightweight aggregates: correlation between molecular/pore structure and performance. *Constr. Build. Mater.* **2016**, *124*, 485−495.
(27) Brinker, C. J.; Scherer, G. W. *Sol-Gel Science: The Physics and Chemistry of Sol-Gel Processing*; Academic Press: New York, 1990; pp 25−29.
(28) Seguin, K.; Dallas, A. J.; Weineck, G. Rationalizing the mechanism of HMDS degradation in air and effective control of the reaction byproducts. *Proc. SPIE* **2008**, *6922*, 692230.
(29) Hair, M. L.; Hertl, W. Reaction of hexamethyldisilazane with silica. *J. Phys. Chem.* **1971**, *75*, 2181−2185.
(30) Gun'ko, V. M.; Vedamuthu, M. S.; Henderson, G. L.; Blitz, J. P. Mechanism and kinetics of hexamethyldisilazane reaction with a fumed silica surface. *J. Colloid Interface Sci.* **2000**, *228*, 157−170.
(31) Nakamoto, K. *Infrared and Raman Spectra of Inorganic and Coordination Compounds: Part A: Theory and Applications in Inorganic Chemistry*, 5th ed.; Wiley: New York, 1997; pp 195−197.
(32) Bellamy, L. J. *The Infrared Spectra of Complex Molecules*, 3rd ed.; Chapman and Hall: London, 1975; pp 21−26.
(33) Kamiya, K.; Iwamoto, Y.; Yoko, T.; Sakka, S. Hydrolysis and condensation reactions of $Si(OC_2H_5)_4$ related to silica fiber drawing. *J. Non-Cryst. Solids* **1988**, *100*, 195−200.
(34) Fidalgo, A.; Ilharco, L. M. Chemical tailoring of porous silica xerogels: local structure by vibrational spectroscopy. *Chem.—Eur. J.* **2004**, *10*, 392−398.
(35) Marmur, A.; Della Volpe, C.; Siboni, S.; Amirfazli, A.; Drelich, J. W. Contact angles and wettability: towards common and accurate terminology. *Surf. Innovations* **2017**, *5*, 3−8.
(36) Brunauer, S.; Emmett, P. H.; Teller, E. Adsorption of gases in multimolecular layers. *J. Am. Chem. Soc.* **1938**, *60*, 309−319.
(37) Barrett, E. P.; Joyner, L. G.; Halenda, P. P. The determination of pore volume and area distributions in porous substances. I. Computations from nitrogen isotherms. *J. Am. Chem. Soc.* **1951**, *73*, 373−380.
(38) Sing, K. S. W.; Everett, D. H.; Haul, R. A. W.; Moscou, L.; Pierotti, R. A.; Rouquérol, J.; Siemieniewska, T. Reporting physisorption data for gas/solid systems with special reference to the determination of surface area and porosity. *Pure Appl. Chem.* **1985**, *57*, 603−619.
(39) Kanamori, K. Organic−inorganic hybrid aerogels with high mechanical properties via organotrialkoxysilane-derived sol−gel process. *J. Chem. Soc. Jpn.* **2011**, *119*, 16−22.
(40) Iswar, S.; Malfait, W. J.; Balog, S.; Winnefeld, F.; Lattuada, M.; Koebel, M. M. Effect of aging on silica aerogel properties. *Microporous Mesoporous Mater.* **2017**, *241*, 293−302.
(41) Scherer, G. W. Recent progress in drying of gels. *J. Non-Cryst. Solids* **1992**, *147−148*, 363−374.
(42) Reichenauer, G.; Scherer, G. W. Nitrogen adsorption in compliant materials. *J. Non-Cryst. Solids* **2000**, *277*, 162−172.

DOI: 10.1021/acsomega.7b00893
ACS Omega 2017, 2, 5060−5070